Critical Thermalization of a Disordered Dipolar Spin System in Diamond

G. Kucsko,[1] S. Choi,[1] J. Choi,[1,2] P. C. Maurer,[3] H. Zhou,[1] R. Landig,[1] H. Sumiya,[4] S. Onoda,[5] J. Isoya,[6] F. Jelezko,[7] E. Demler,[1] N. Y. Yao,[8] and M. D. Lukin[1,*]

[1]*Department of Physics, Harvard University, Cambridge, Massachusetts 02138, USA*
[2]*School of Engineering and Applied Sciences, Harvard University, Cambridge, Massachusetts 02138, USA*
[3]*Department of Physics, Stanford University, Stanford, California 94305, USA*
[4]*Sumitomo Electric Industries Ltd., Itami, Hyougo, 664-0016, Japan*
[5]*Takasaki Advanced Radiation Research Institute, National Institutes for Quantum and Radiological Science and Technology, Takasaki, Gunma 370-1292, Japan*
[6]*Research Centre for Knowledge Communities, University of Tsukuba, Tsukuba, Ibaraki 305-8550, Japan*
[7]*Institut für Quantenoptik, Universität Ulm, 89081 Ulm, Germany*
[8]*Department of Physics, University of California Berkeley, Berkeley, California 94720, USA*

(Received 3 January 2018; published 9 July 2018)

Statistical mechanics underlies our understanding of macroscopic quantum systems. It is based on the assumption that out-of-equilibrium systems rapidly approach their equilibrium states, forgetting any information about their microscopic initial conditions. This fundamental paradigm is challenged by disordered systems, in which a slowdown or even absence of thermalization is expected. We report the observation of critical thermalization in a three dimensional ensemble of $\sim 10^6$ electronic spins coupled via dipolar interactions. By controlling the spin states of nitrogen vacancy color centers in diamond, we observe slow, subexponential relaxation dynamics and identify a regime of power-law decay with disorder-dependent exponents; this behavior is modified at late times owing to many-body interactions. These observations are quantitatively explained by a resonance counting theory that incorporates the effects of both disorder and interactions.

DOI: 10.1103/PhysRevLett.121.023601

Nearly six decades ago, Anderson predicted that the interplay between long-range couplings and disorder in quantum systems can lead to a novel regime of slow, subdiffusive thermalization [1]. This is in stark contrast to both conventional ergodic systems and disordered systems with short-range hopping, where disorder can arrest dynamics, resulting in the breakdown of ergodicity. Termed Anderson localization, the latter effect has been observed in systems ranging from acoustic and optical waves to cold atomic gases [2–4]; more recently, it has been shown that localization can persist even in strongly interacting, isolated quantum systems, a phenomenon dubbed many-body localization [5–7]. In addition to raising fundamental questions, such systems have also become a basis for the exploration of novel nonequilibrium phases of matter, including Floquet symmetry protected topological phases [8] and discrete time crystals [9,10].

The addition of long-range couplings tends to facilitate delocalization, leading to a regime where ergodicity and localization compete [11,12]. This so-called critical regime is realized by dipolar spins in three dimensions, where a combination of power-law interactions, dimensionality, and disorder govern the microscopic dynamics [1,13,14]. Such systems have long been explored in the context of nuclear magnetic resonance spectroscopy, where a wide variety of techniques have been developed to effectively engineer and control spin dynamics [15–19]. Despite this, the direct observation of slow, critical dynamics in the presence of strong, controllable disorder remains an outstanding challenge, owing to difficulties in preparing a low-entropy spin state, such as a polarized initial state.

In this Letter, we report the observation of critical dynamics using disordered, strongly interacting electronic spin impurities associated with nitrogen-vacancy (NV) centers in diamond. More specifically, we study the thermalization of an initially polarized spin ensemble coupled to a bath of unpolarized spins [Fig. 1(a)] and quantitatively explain its dynamics using a resonance counting theory. Each NV center constitutes an $S = 1$ spin system with three internal states $|m_s = \pm 1\rangle$ and $|m_s = 0\rangle$, which can be initialized, manipulated, and optically read out under ambient conditions [Figs. 1(b)–1(c)]. In our experiments, we utilize a dense ensemble of NV centers, where the average NV-to-NV separation of 5 nm leads to strong dipolar interaction strength $J \sim (2\pi)420$ kHz, a significantly faster timescale than typical spin coherence times [20,22]. The diamond sample was fabricated from a high-pressure high-temperature type-Ib natural abundance (^{13}C 1.1%) diamond with an initial nitrogen concentration of 100 ppm. Using high fluence electron irradiation and

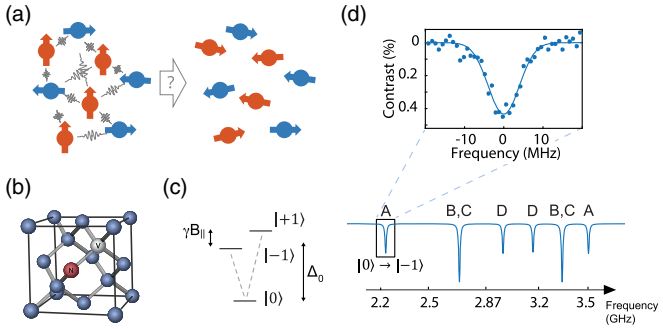

FIG. 1. Experimental system. (a) Schematic depicting two groups of spin ensembles interacting via long-range dipolar interactions. An initially polarized system (red arrows) coupled to a bath of unpolarized spins (blue arrows) will eventually thermalize to an unpolarized spin state. (b) The crystallographic structure of diamond contains four possible NV quantization axes. (c) Simplified NV level scheme showing the spin degrees of freedom in the optical ground state. A large zero-field splitting $\Delta_0 = (2\pi)2.87$ GHz in combination with a magnetic field induced Zeeman shift $\gamma B_{\parallel}$ leads to individual addressability of the spin sublevels. (d) The lower image shows a simulated ESR scan, revealing the spin transitions of all four NV groups $\{A, B, C, D\}$. The upper figure shows an ESR scan of a single transition of NV spins (blue points). Blue solid line represents a Gaussian fit with standard deviation W, corresponding to the average disorder in the sample.

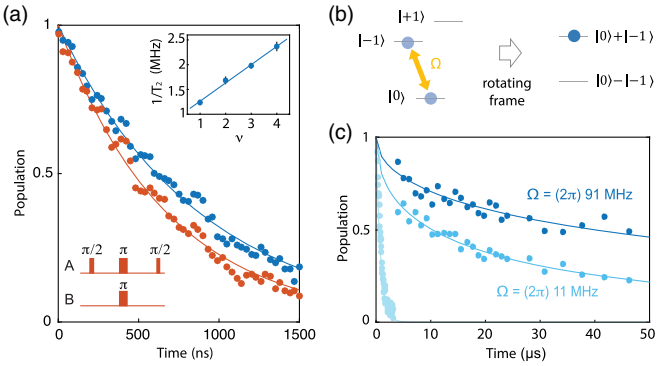

FIG. 2. Interacting spin ensemble. (a) Spin echo on NV group A (blue points) and DEER scan on groups A and B (red points). The bottom left inset illustrates the DEER pulse sequence. Solid lines indicate exponential fits to the data. The inset shows the spin echo coherence time as a function of resonant NV groups (blue points). The blue solid line represents a linear fit to the data. (b) Schematic depicting the NV level scheme during a spin-lock sequence. (c) Spin-lock coherence decay for low (light-blue points) and high (dark blue points) cw driving strength, showing significant extension beyond the spin echo decoherence (gray-blue points). The decay curves are fitted to a stretched exponential function $\exp\left[-\sqrt{t/T}\right]$ [23].

in situ annealing, an NV center concentration of 45 ppm was achieved [20]. Electron spin resonance (ESR) measurements reveal that our sample is also characterized by a strong on-site potential disorder $W \approx (2\pi)4.0$ MHz [Fig. 1(d)] caused by an abundance of paramagnetic impurities as well as strain in the diamond lattice [20].

NV centers are oriented along four different crystallographic axes of the diamond lattice. Different projections of an external magnetic field naturally lead to distinct energy splittings and define four unique NV groups, $\{A, B, C, D\}$, which can be individually addressed and controlled in a finite B field via resonant microwave radiation. By tuning the direction of the magnetic field, one can modify the number of spectrally overlapping groups and hence the effective density of spins [Fig. 1(d)]. To directly probe the interaction strength within our system, we perform a double electron-electron resonance (DEER) measurement between two spectrally separated NV groups, A and B [Fig. 2(a), bottom inset]. In this measurement the spin echo protocol decouples group A from slowly varying magnetic noise. However, the additional π pulse on group B after half of the total evolution ensures that the dephasing induced by interactions between the two groups is not decoupled. As depicted in Fig. 2(a), this measurement allows us to extract the interaction strength $\sim(2\pi)420$ kHz [20]. By tuning additional NV groups into spectral resonance, we can confirm that the spin dynamics are dominated by interactions. As a function of the number of resonant groups, ν, we find a total dephasing rate, $\gamma_T = \gamma_b + \nu\gamma_0$, with $\gamma_b \approx 0.9$ and $\gamma_0 \approx 0.4$ MHz, consistent with 45 ppm NV center density [Fig. 2(a) inset] [20]. The linear dependence of γ_T on ν suggests that the dephasing is dominated by coherent interactions, whose strength is proportional to the density of resonant NV groups. The extracted $\gamma_b \approx 0.9$ MHz, a bare decoherence rate, could originate partly from the interactions with single nitrogen defects (P1 centers).

Central to our thermalization experiments is the ability to tune both the disorder strength and interactions. This is achieved by using spin-locking and Hartmann-Hahn (HH) resonances, both of which rely upon continuous microwave driving resonant with the $|m_s = 0\rangle \rightarrow |m_s = -1\rangle$ transitions of the respective NV groups [24,25]. For excitation with Rabi frequency Ω, this defines a "dressed-state" basis, $|\pm\rangle \approx (|m_s = 0\rangle \pm |m_s = -1\rangle)/\sqrt{2}$ [Fig. 2(b)]. In the rotating frame, the energies of these two states are split by the effective on-site potential $\sqrt{\Omega^2 + \delta_i^2}$, where δ_i is the local disorder potential for spin i (of order W). In the limit of strong driving $\Omega \gg \delta_i$, we obtain an effective disorder potential $\tilde{\delta}_i$ with the reduced width $W_{\text{eff}} \sim W^2/\Omega$, allowing us to tune the disorder by simply adjusting the Rabi frequency. For spin locking, we initially polarize NVs in the dressed-state basis. After an evolution time τ the polarization can be converted back to the bare basis, yielding a dramatic enhancement of the lifetime compared to a spin-echo measurement [Fig. 2(c)]. We find that the lifetime is limited by interactions with short-lived spins in our system, which are suppressed by increasing Ω [23]. Thus, spin locking enables us to prepare a single

group of polarized NVs with tunable disorder and long lifetime.

To control interactions, we utilize a HH resonance permitting cross-polarization transfer between two spin ensembles [24,25]. To this end we align the 160 G magnetic field along the $[1, \bar{2}, \bar{3}]$ direction, which allows groups A and B to be spectrally distinguished, and at the same time, to be isolated from the groups C and D by a detuning larger than all relevant Rabi frequencies. Within this setting, we prepare two oppositely polarized spin ensembles in the dressed-state basis with energy splittings Ω_A and Ω_B [Fig. 3(a)]. Figure 3(b) depicts the results of a spin-lock measurement on group A as a function of Ω_B, revealing a sharp resonance with a linewidth significantly narrower than the on-site disorder strength W. The linewidth of this resonance can be monitored as a function of the common Rabi frequency $\Omega = \Omega_A = \Omega_B$, showing a strong decrease for higher Ω caused by a reduction of the effective disorder W_{eff} [Fig. 3(b) inset].

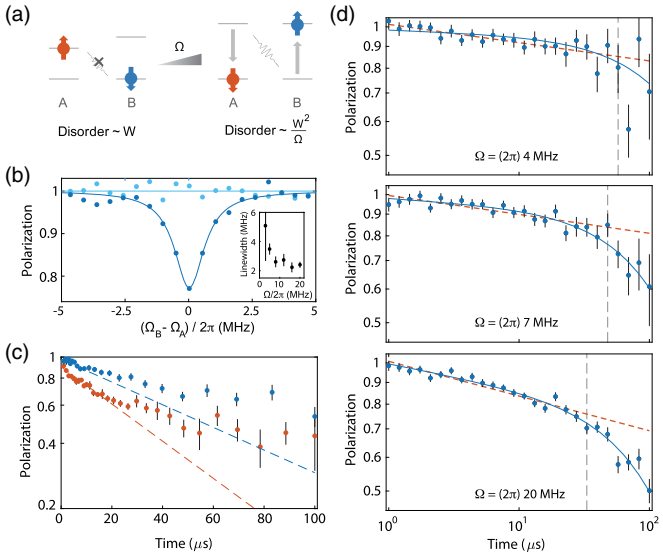

FIG. 3. Spin cross relaxation. (a) Schematic depicting two oppositely polarized groups of spins (A and B) in the dressed-state basis. Under spin locking with a common Rabi frequency Ω, the effective disorder reduces from the natural disorder W with increasing Ω, thereby enhancing the rate of resonant spin exchange. (b) Population of group A as a function of driving strength of group B, showing the HH resonance (dark blue points). Light blue data show spin-lock coherence without driving of other groups. The corresponding solid curves represent a Lorentzian and constant fit to the data. Inset shows the HH resonance linewidth as a function of applied Rabi frequency. (c) Polarization dynamics of group A interacting with an oppositely polarized (red) and unpolarized (blue) spin bath, group B, at the HH condition with $\Omega = (2\pi)9$ MHz as a function of evolution time. The polarized spin bath leads to faster polarization decay [20]. Dashed lines represent an exponential decay, showing significant deviation at long times. (d) Polarization decay of group A under HH conditions with unpolarized group B for different driving strengths. Dashed red lines are power-law fits to the data in the time window up to the vertical line. Curved solid lines are the fits to our theory model including time-dependent disorder. All error bars correspond to 1σ.

This method allows us to probe the thermalization dynamics with controlled interaction and tunable disorder. To this end, we investigate the dynamics of an initially polarized spin subensemble (group A) in HH resonance with another, unpolarized subensemble (group B). Physically, this situation corresponds to the thermalization of a polarized spin ensemble in contact with a spin bath held at infinite effective temperature. To extract the coherent thermalization dynamics, we normalize the polarization decay with a sufficiently detuned HH measurement [20], wherein we observe a decay profile that fits neither a diffusive power law ($\sim t^{3/2}$) nor a simple exponential [Fig. 3(c)]. By varying the driving strength Ω, we find that the polarization decays faster for larger Ω, consistent with a smaller effective disorder [Fig. 3(d)]. Interestingly, the functional profiles of the decays are consistent with power laws for over a decade, followed by accelerated relaxation at late times.

To understand these observations, we turn to a theoretical description of our system. Spin dynamics are governed by the interplay between disorder and long-range dipolar interactions. Working in the dressed-state basis, we find that the form of this interaction depends on whether spins reside in the same or in distinct groups. For spins in different groups (A and B), dipolar interactions naturally lead to spin exchange. However, for spins in the same group, the $S = 1$ nature of the NV centers and energy conservation in the rotating frame lead to an absence of spin exchange [20]; rather, the coupling between spins takes the form of an Ising interaction. Thus, when initially polarized, a spin may depolarize only through exchange with spins of the other group. Specifically, in the limit of strong disorder, one expects the dynamics to be dominated by rare resonant exchange processes between the two groups. To describe such dynamics, we consider a simplified model, where a single group A excitation is located at the center of an ensemble of group B spins [Fig. 4(a)]. The dynamics of this excitation are captured by an effective Hamiltonian,

$$H_{\text{eff}} = \sum_i \tilde{\delta}_i \sigma_i^x - \sum_{ij} \frac{J_{ij}}{r_{ij}^3} (\sigma_i^+ \sigma_j^- + \text{H.c.}), \qquad (1)$$

where r_{ij} is the distance between spins, J_{ij} is the orientation dependent coefficient of the dipolar interaction with typical strength $J_0 = (2\pi)52\ \text{MHz}\,\text{nm}^3$, $\vec{\sigma}$ are spin-1/2 operators with $\sigma_i^{\pm} = \sigma_i^y \pm i\sigma_i^z$, and $\tilde{\delta}_i = \sqrt{\Omega^2 + \delta_i^2} - \Omega$ is the effective quenched disorder potential. While this single-particle model neglects the many-body nature of our experiments such as intragroup Ising interactions and complex dynamics of group B excitations, it captures the key features of slow relaxation in critical systems; however, these additional features will be necessary to accurately describe the long time thermalization behavior as discussed later.

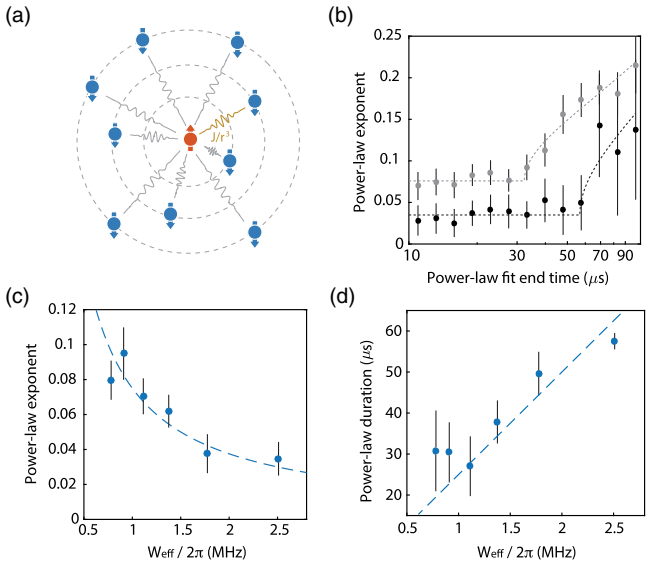

FIG. 4. Understanding thermalization dynamics. (a) Schematic of single particle resonance counting argument predicting a power-law decay profile. (b) Variation of power-law exponents extracted from a subset of data, consisting of seven subsequent points, swept from the beginning to the end of thermalization time traces. Black and gray data correspond to the case of $\Omega = (2\pi)4$ and 9 MHz, respectively. Dotted lines correspond to phenomenological fits, identifying the duration over which the power-law exponents remain constant. (c) Power-law decay exponents of group A polarization as a function of effective disorder W_{eff}. Dashed line corresponds to a theoretical prediction based on the single particle resonance counting. (d) Duration of power-law dynamics extracted for various strengths of effective disorder W_{eff}. Dashed line corresponds to a theoretical prediction based on a refined resonance counting including time-dependent disorder. All error bars correspond to 1σ.

To characterize the spin decay dynamics governed by H_{eff}, we calculate the survival probability $P(t)$ of the excitation via a simple resonance counting analysis. For a given disorder realization, this resonance counting proceeds as follows. Two spins at sites i and j are on resonance at time t if (i) their energy mismatch is smaller than their dipolar interaction strength, $|\tilde{\delta}_i - \tilde{\delta}_j| < \beta J_0/r_{ij}^3$ (β is a dimensionless constant of order unity), and (ii) the interaction occurs within the timescale t, $J_{ij}/r_{ij}^3 > 1/t$. $P(t)$ is approximately given by the probability of having found no resonances up to time t or, equivalently, up to distance $R(t) \equiv (J_0 t)^{1/3}$ [20]. This probability can be computed as the product of probabilities of having no resonant spins at any r,

$$P(t) = \prod_{r}^{R(t)} \left(1 - 4\pi n r^2 dr \frac{\beta J_0/r^3}{W_{\text{eff}}}\right) \propto t^{(-4\pi n\beta J_0/3W_{\text{eff}})}. \quad (2)$$

$P(t)$ exhibits power-law decay with a disorder dependent exponent $\eta = 4\pi n\beta J_0/(3W_{\text{eff}})$, where n is the density of spins that are oppositely polarized to the central excitation. This subexponential relaxation is the essence of the slow critical dynamics predicted by Anderson [1]. Such single-particle power-law relaxation is also consistent with results obtained from random-banded matrix theory [14,26] and is numerically verified for up to $N = 10^4$ spins [20].

A detailed comparison of our experimental observations with these theoretical predictions is summarized in Fig. 4. In order to quantify the slow dynamics, we take subsets of our depolarization time trace over half-decade windows, fit the data to power laws, and extract the resulting exponents. Varying the starting time of the windows, we find that the extracted exponents remain constant up to a long time $T^* \gg 1/J$, beyond which they increase, indicating the deviation of the thermalization dynamics from a simple single-particle prediction [Fig. 4(b)]. Interestingly, the exponents scale linearly with the inverse effective disorder, as predicted by the counting argument [Fig. 4(c)]. Furthermore, we find that their values are in excellent agreement with our theory based on numerical simulations of a single-particle Hamiltonian [20].

At late times ($t > T^*$), the observed decay accelerates and deviates significantly from the power law. This is natural since the effects of multiparticle interactions cannot be neglected when a significant fraction of spins have already undergone depolarization. In particular, intragroup Ising interactions among randomly positioned spins $\delta_i^I \equiv \sum_j J_{ij}/r_{ij}^3 \langle \sigma_j^x \rangle$ may behave as an additional disorder that changes in time with characteristic strength $J/4 \sim (2\pi)105$ kHz. Additionally, weak coupling to the environment may also give rise to corrections to our single particle model.

To understand this behavior, we extend our theory analysis by allowing the on-site disorder to vary slowly in time. More specifically, we assume that the disorder potential consists of both static and dynamical parts with standard deviations W_s and W_d, and that the dynamical part changes over a correlation time τ_d. Repeating our previous analysis incorporating the effect of dynamical disorder, we obtain a modified survival probability $\tilde{P}(t) \propto e^{-t/T^*} t^{-\eta}$ with $T^* \equiv 3W_s\tau_d/(4\pi n\beta J_0)$ [20]. The rate $1/T^*$ thus characterizes the deviation from the power-law regime, and can be intuitively understood as the rate at which a pair of initially off-resonant spins comes into resonance as the local potentials vary in time. Figure 3(d) shows that $\tilde{P}(t)$ provides an excellent fit to our observation over all timescales. Both extracted parameters $W_d \sim (2\pi)0.5$ MHz and $\tau_d \sim 40$ μs are comparable to the strength of Ising interactions and independently measured NV depolarization time, respectively [20,23]. This suggests that the dynamical disorder is dominated by intrinsic contributions from Ising interactions, which is related to the predicted thermalization enhancement due to multi-particle resonances and higher order processes [11,12]. Moreover, the extracted power-law duration agrees well with the predicted linear dependence of T^* on effective disorder strengths [Fig. 4(d)]. Together, these observations strongly corroborate our theoretical model describing the microscopic mechanism of thermalization dynamics in a critical system.

We have demonstrated that dense ensembles of NV centers constitute a powerful platform for exploring quantum dynamics of strongly correlated many-body systems. Complementary to recent studies of localization in cold atomic systems [6,7], these spin systems exhibit slow, disorder-dependent relaxation associated with critical thermalization dynamics. The quantitative agreement between the observed spin relaxation and resonance counting theory demonstrates that the dynamics are dominated by rare resonances. Moreover, the observed deviations from single-particle theory reveal the subtle role that many-body effects can play in such systems. These studies can be extended along several directions. A higher degree of spatial quantum control can be obtained via spin-based subwavelength imaging techniques [27]. Advanced dynamical decoupling can enable the engineering of a broader class of interaction Hamiltonians and the direct measurement of quantum entanglement dynamics [28,29]. The use of strong magnetic field gradients or the fabrication of diamond nanostructures can allow for the exploration of spin dynamics in lower dimensional systems [30], where the existence of many-body localization is still in debate [11,13]. In combination, these directions may enable the study of dynamical phase transitions from localization to thermalization [6,31,32] as well as exotic nonequilibrium phases of matter [8–10].

We thank A. Gali, D. Budker, B. J. Shields, A. Sipahigil, M. Knap, S. Gopalakrishnan, and J. Chalker for insightful discussions and N. P. De Leon for fabricating the diamond nanobeam. This work was supported in part by CUA, NSSEFF, ARO MURI, Moore Foundation, Miller Institute for Basic Research in Science, Kwanjeong Educational Foundation, Samsung Fellowship, NSF PHY-1506284, NSF DMR-1308435, Japan Society for the Promotion of Science KAKENHI (No. 26246001), EU (FP7, Horizons 2020, ERC), DFG, SNF, Volkswagenstiftung, and BMBF.

G. K., S. C., and J. C., contributed equally to this work.

*To whom correspondence should be addressed.
lukin@physics.harvard.edu.

[1] P. W. Anderson, Phys. Rev. **109**, 1492 (1958).
[2] T. Schwartz, G. Bartal, S. Fishman, and M. Segev, Nature (London) **446**, 52 (2007).
[3] J. Billy, V. Josse, Z. Zuo, A. Bernard, B. Hambrecht, P. Lugan, D. Clément, L. Sanchez-Palencia, P. Bouyer, and A. Aspect, Nature (London) **453**, 891 (2008).
[4] G. Roati, C. DErrico, L. Fallani, M. Fattori, C. Fort, M. Zaccanti, G. Modugno, M. Modugno, and M. Inguscio, Nature (London) **453**, 895 (2008).
[5] R. Nandkishore and D. A. Huse, Annu. Rev. Condens. Matter Phys. **6**, 15 (2015).
[6] M. Schreiber, S. S. Hodgman, P. Bordia, H. P. Lüschen, M. H. Fischer, R. Vosk, E. Altman, U. Schneider, and I. Bloch, Science **349**, 842 (2015).
[7] J. Smith, A. Lee, P. Richerme, B. Neyenhuis, P. W. Hess, P. Hauke, M. Heyl, D. A. Huse, and C. Monroe, Nat. Phys. **12**, 907 (2016).
[8] A. C. Potter, T. Morimoto, and A. Vishwanath, Phys. Rev. X **6**, 041001 (2016).
[9] J. Zhang, P. W. Hess, A. Kyprianidis, P. Becker, A. Lee, J. Smith, G. Pagano, I. D. Potirniche, A. C. Potter, A. Vishwanath, N. Y. Yao, and C. Monroe, Nature (London) **543**, 217 (2017).
[10] S. Choi, J. Choi, R. Landig, G. Kucsko, H. Zhou, J. Isoya, F. Jelezko, S. Onoda, H. Sumiya, V. Khemani *et al.*, Nature (London) **543**, 221 (2017).
[11] A. L. Burin, arXiv:cond-mat/0611387.
[12] N. Y. Yao, C. R. Laumann, S. Gopalakrishnan, M. Knap, M. Müller, E. A. Demler, and M. D. Lukin, Phys. Rev. Lett. **113**, 243002 (2014).
[13] L. S. Levitov, Phys. Rev. Lett. **64**, 547 (1990).
[14] V. E. Kravtsov, O. M. Yevtushenko, P. Snajberk, and E. Cuevas, Phys. Rev. E **86**, 021136 (2012).
[15] C. P. Slichter, *Principles of Magnetic Resonance* (Springer Science & Business Media, New York, 2013), Vol. 1.
[16] A. J. Vega, J. Magn. Reson. **65**, 252 (1985).
[17] P. Robyr, B. Meier, and R. Ernst, Chem. Phys. Lett. **162**, 417 (1989).
[18] X. Wu and S. Zhang, Chem. Phys. Lett. **156**, 79 (1989).
[19] S. Zhang, B. H. Meier, and R. R. Ernst, Phys. Rev. Lett. **69**, 2149 (1992).
[20] See Supplemental Material at http://link.aps.org/supplemental/10.1103/PhysRevLett.121.023601 for details about sample characterization, experimental techniques, data analysis, and theoretical models, which includes Ref. [21].
[21] E. Van Oort and M. Glasbeek, Chem. Phys. Lett. **168**, 529 (1990).
[22] G. Balasubramanian, P. Neumann, D. Twitchen, M. Markham, R. Kolesov, N. Mizuochi, J. Isoya, J. Achard, J. Beck, J. Tissler *et al.*, Nat. Mater. **8**, 383 (2009).
[23] J. Choi, S. Choi, G. Kucsko, P. C. Maurer, B. J. Shields, H. Sumiya, S. Onoda, J. Isoya, E. Demler, F. Jelezko, N. Y. Yao, and M. D. Lukin, Phys. Rev. Lett. **118**, 093601 (2017).
[24] S. Hartmann and E. Hahn, Phys. Rev. **128**, 2042 (1962).
[25] C. Belthangady, N. Bar-Gill, L. M. Pham, K. Arai, D. Le Sage, P. Cappellaro, and R. L. Walsworth, Phys. Rev. Lett. **110**, 157601 (2013).
[26] A. D. Mirlin, Y. V. Fyodorov, F.-M. Dittes, J. Quezada, and T. H. Seligman, Phys. Rev. E **54**, 3221 (1996).
[27] P. Maurer, J. Maze, P. Stanwix, L. Jiang, A. V. Gorshkov, A. A. Zibrov, B. Harke, J. Hodges, A. S. Zibrov, A. Yacoby *et al.*, Nat. Phys. **6**, 912 (2010).
[28] P. Hauke, M. Heyl, L. Tagliacozzo, and P. Zoller, Nat. Phys. **12**, 778 (2016).
[29] S. Choi, N. Y. Yao, and M. D. Lukin, Phys. Rev. Lett. **119**, 183603 (2017).
[30] M. J. Burek, N. P. de Leon, B. J. Shields, B. J. Hausmann, Y. Chu, Q. Quan, A. S. Zibrov, H. Park, M. D. Lukin, and M. Loncar, Nano Lett. **12**, 6084 (2012).
[31] T. Langen, S. Erne, R. Geiger, B. Rauer, T. Schweigler, M. Kuhnert, W. Rohringer, I. E. Mazets, T. Gasenzer, and J. Schmiedmayer, Science **348**, 207 (2015).
[32] E. Kaminishi, T. Mori, T. N. Ikeda, and M. Ueda, Nat. Phys. **11**, 1050 (2015).